

# Competing effects of Hund's splitting and symmetry-breaking perturbations on electronic order in $\text{Pb}_{1-x}\text{Sn}_x\text{Te}$

Sarbajaya Kundu and Vikram Tripathi

*Department of Theoretical Physics, Tata Institute of Fundamental Research,  
Homi Bhabha Road, Navy Nagar, Colaba, Mumbai-400005,*

(Dated: September 8, 2017)

We study the effect of a uniform external magnetization on  $p$ -wave superconductivity on the (001) surface of the crystalline topological insulator (TCI)  $\text{Pb}_{1-x}\text{Sn}_x\text{Te}$ . It was shown by us in an earlier work that a chiral  $p$ -wave finite-momentum pairing (FFLO) state can be stabilized in this system in the presence of weak repulsive interparticle interactions. In particular, the superconducting instability is very sensitive to the Hund's interaction in the multiorbital TCI, and no instabilities are found to be possible for the "wrong" sign of the Hund's splitting. Here we show that for a finite Hund's splitting of interactions, a significant value of the external magnetization is needed to degrade the surface superconductivity, while in the absence of the Hund's interaction, an arbitrarily small external magnetization can destroy the superconductivity. This implies that multiorbital effects in this system play an important role in stabilizing electronic order on the surface.

The topological crystalline insulator (TCI) [1] phase is a new state of matter where the topological character of the electronic bands is protected by crystalline symmetries. The IV-VI semiconductors  $\text{SnTe}$  and related semiconducting alloys  $\text{Pb}_{1-x}\text{Sn}_x(\text{Te,Se})$  were recently predicted to belong to the TCI class [2–5]. These have an even number of Dirac cones on high-symmetry crystal surfaces such as  $\{001\}$ ,  $\{110\}$  and  $\{111\}$ , topologically protected by the reflection symmetry with respect to the  $\{110\}$  mirror planes. Here the nontrivial topology is mathematically characterized by a mirror Chern number [3], and topologically protected surface states with novel electronic dispersions are present on the different surfaces invariant under reflection symmetry. In particular, it has been shown in [6] that the (001) surface of  $\text{Pb}_{1-x}\text{Sn}_x\text{Te}$  comprises two disconnected Dirac pockets touching each other at two saddle points, giving rise to Type-II Van-Hove singularities [7] in the density of states. This enhances the possibility of competing Fermi-surface instabilities on the TCI surface, brought about by weak repulsive interparticle interactions [8–14].

In order to study the competition between different electronic orders, a weak-coupling renormalization group analysis, which treats all the competing orders on an equal footing, is desirable. Such a parquet approximation for systems with multiple Fermi pockets has proved useful in the past for studies on unconventional superconductivity [15–17] in multiple other systems such as cuprates [18], graphene [19] and semimetal thin films [20]. In the presence of Fermi surface nesting, charge and spin density wave orders tend to compete with superconductivity [21]. In a multiorbital system like  $\text{Pb}_{1-x}\text{Sn}_x\text{Te}$ , one also has to take into account the effect of Hund's splitting of repulsive electron interactions. We have shown in an earlier work [22] that the electrons interacting via repulsive interactions on the TCI surface are unstable against a chiral  $p$ -wave superconducting order, where the Van-Hove singularities serve to enhance the effective transi-

tion temperature and the (approximate) nesting allows the particle-hole instabilities to compete with superconductivity on an equal footing. Interestingly, here the  $p$ -wave symmetry arises not from intrinsic Fermi-surface deformations but from the nontrivial Berry phases associated with the topological surface states. Moreover, the very existence of the superconducting state is sensitive to the Hund's interaction in this system and no instabilities are found to occur for a negative Hund's splitting. Due to the presence of the low-lying Van-Hove singularities on the TCI surface, such a state promises to be experimentally accessible.

A relevant question which ought to be addressed in this context is: how robust is such a superconducting order against a time-reversal symmetry breaking perturbation, such as proximity coupling to an external magnetization. The effects of various symmetry-breaking perturbations, including a perpendicular magnetic field or moments, on the surface states of the TCI (as well as other topological insulators) have been studied both theoretically and experimentally [23–27]; however, here we focus on an aspect of the system that has been previously overlooked. We show that the robustness of the surface superconducting order against an external magnetization is enhanced by the presence of a finite Hund's interaction. Specifically, the critical value of spin-splitting (induced by the magnetization), beyond which  $p$ -wave superconductivity is no longer possible, scales directly with the size of the Hund's splitting with respect to the repulsive electron interaction strength. This implies that multiorbital effects in this system play an important role in stabilizing electronic order on the surface.

The rest of the paper is organized as follows. In Sec. 1, we introduce the  $k.p$  Hamiltonian for the (001) surface and describe some of the features of eigenstates and the spectrum in the presence of a spin-splitting term. Sec. 2 presents the low-energy theory for weakly repulsive electronic interactions, including a finite Hund's splitting. In

Sec. 3, the parquet renormalization group equations for the couplings are provided. In Sec. 4, we solve the renormalization group equations and obtain the singular behavior of different susceptibilities near the critical point. Sec. 5 is devoted to situations where the parquet analysis is no longer valid (if the parquet fixed point corresponds to an energy scale below the Fermi surface) for which we perform the usual ladder renormalization group analysis and obtain the instabilities in the system. In Sec. 6, we determine the behavior of the critical values of spin-splitting below which  $p$ -wave superconductivity is stable in the presence of a finite Hund's interaction, as a function of the Hund's splitting introduced. Sec. 7 contains a summary of our results and a discussion.

## 1. THE SURFACE HAMILTONIAN AND TWO-DIMENSIONAL VAN-HOVE SINGULARITIES

The fundamental band gaps of IV-VI semiconductors are located at the four equivalent  $L$  points in the FCC Brillouin zone. According to [6], the TCI surface states can be classified into two types: *Type-I*, for which all four  $L$ -points are projected to the different time-reversal invariant momenta (TRIM) in the surface Brillouin zone, and *Type-II*, for which different  $L$ -points are projected to the same surface momentum. The (001) surface falls into the latter class of surfaces. Here, the plane  $\Gamma L_1 L_2$  in the bulk Brillouin zone projects onto the line  $\overline{\Gamma X_1}$  on the surface, such that  $L_1$  and  $L_2$  both project onto the  $\overline{X_1}$  point. Similarly,  $L_3$  and  $L_4$  project onto the symmetry-related point  $\overline{X_2}$ . This leads to two coexisting massless Dirac fermions at  $\overline{X_1}$  arising from the  $L_1$  and the  $L_2$  valley, respectively, and likewise at  $\overline{X_2}$ . The k.p Hamiltonian close to the point  $\overline{X_1}$  on the (001) surface is derived on the basis of a symmetry analysis in [6], and is given by

$$H_{\overline{X_1}}(k) = (v_x k_x s_y - v_y k_y s_x) + m\tau_x + \delta s_x \tau_y, \quad (1)$$

where  $k$  is measured with respect to  $\overline{X_1}$ ,  $\tau$  operates in valley ( $L$ ) space and  $\vec{s}$  is a set of Pauli matrices associated with the two spin components associated with each valley, and the terms  $m$  and  $\delta$  are added to describe intervalley scattering. The band dispersion and constant energy contours for the above surface Hamiltonian undergo a Lifshitz transition with increasing energy away from the Dirac point, and when the Fermi surface is at  $\sim 26$  meV [6], two saddle points  $\overline{S_1}$  and  $\overline{S_2}$  at momenta  $(\pm \frac{m}{v_x}, 0)$  lead to a Van-Hove singularity in the density of states. A similar situation arises at the point  $\overline{X_2}$ . This is illustrated in Fig. 1(a). Here we further introduce a spin-splitting term  $M s_z$  into the surface Hamiltonian in Eq. 1, which breaks the degeneracy between the two spin components. The authors of ref. [23] have also incorporated additional terms (involving the valley degrees of freedom)

to describe the Zeeman coupling of the TCI surface states to a perpendicular magnetic field or magnetic moment, deduced on the basis of a symmetry analysis of the surface Hamiltonian. We have repeated our calculations for their model and find that the results change only quantitatively, and hence, we shall consider the simpler case with a Zeeman-only perturbation. We find that the Van-Hove singularities in the surface bandstructure survive up to  $M \approx 0.05$  eV (with parameters suitable for SnTe being taken from [6]), when the Fermi level is at  $\approx 0.026$  eV, the position of the Van-Hoves in the absence of  $M$ . The evolution of the two-dimensional Van-Hove singularities with an increase in the Zeeman splitting  $M$  is shown in the Fig. 1. The TCI surface is found to have a chiral spin texture in the absence of an external magnetization, and as  $M$  ( $>0$ ) increases, it acquires an out-of-plane spin polarization. This is graphically depicted in Fig. 2. The topological defects are visible at the  $\overline{X}$  point.

## 2. ELECTRON INTERACTIONS IN THE VALLEY-SPIN BASIS AND FORM FACTORS

In addition to the noninteracting Hamiltonian with an external magnetization, described in the previous section, we also consider interactions between electrons on different  $L$ -valleys for different spin combinations. We then project the interactions in the valley-spin basis to the positive energy band lying closest to the Van-Hove singularities (corresponding to each of the  $\overline{X}$  points) where the Fermi level is fixed, and this gives rise to additional form factors in the different interaction terms. We find that the form factors  $u_{a\uparrow}$  corresponding to the spin  $\uparrow$  component (for each valley  $a$ ) have an additional phase factor of  $\exp[i\theta_k]$  where  $\theta_k$  is measured with respect to the  $\overline{X}$  point, and the argument of the form factors  $u_{a\downarrow}$  for the spin  $\downarrow$  components do not change upon advancing by  $2\pi$  around the  $\overline{X}$  point. Upon substituting the appropriate form factors into the electron interaction model in the valley-spin basis, the low-energy theory for the effective interaction model in the band picture is given by (please refer to [22] for details)

$$L = \sum_{i,\sigma,\sigma'} \left[ \psi_i^\dagger (\partial_\tau - \epsilon_k + \mu) \psi_i - \frac{1}{2} h_4^{\sigma\sigma'} \psi_i^\dagger \psi_i^\dagger \psi_i \psi_i \right. \\ \left. - \sum_{i \neq j} \frac{1}{2} (h_1^{\sigma\sigma'} \psi_i^\dagger \psi_j^\dagger \psi_i \psi_j + h_2^{\sigma\sigma'} \psi_i^\dagger \psi_j^\dagger \psi_j \psi_i \right. \\ \left. + h_3^{\sigma\sigma'} \psi_i^\dagger \psi_i^\dagger \psi_j \psi_j \right], \quad (2)$$

where the summation  $i$  is over the two bands (corresponding to the two points  $\overline{X_1}$  and  $\overline{X_2}$ ) being considered. Here,  $\epsilon_k$  is obtained by diagonalizing Eq. 1, along with the spin-splitting term  $M s_z$ . The chemical potential value  $\mu=0$  corresponds to the system being doped

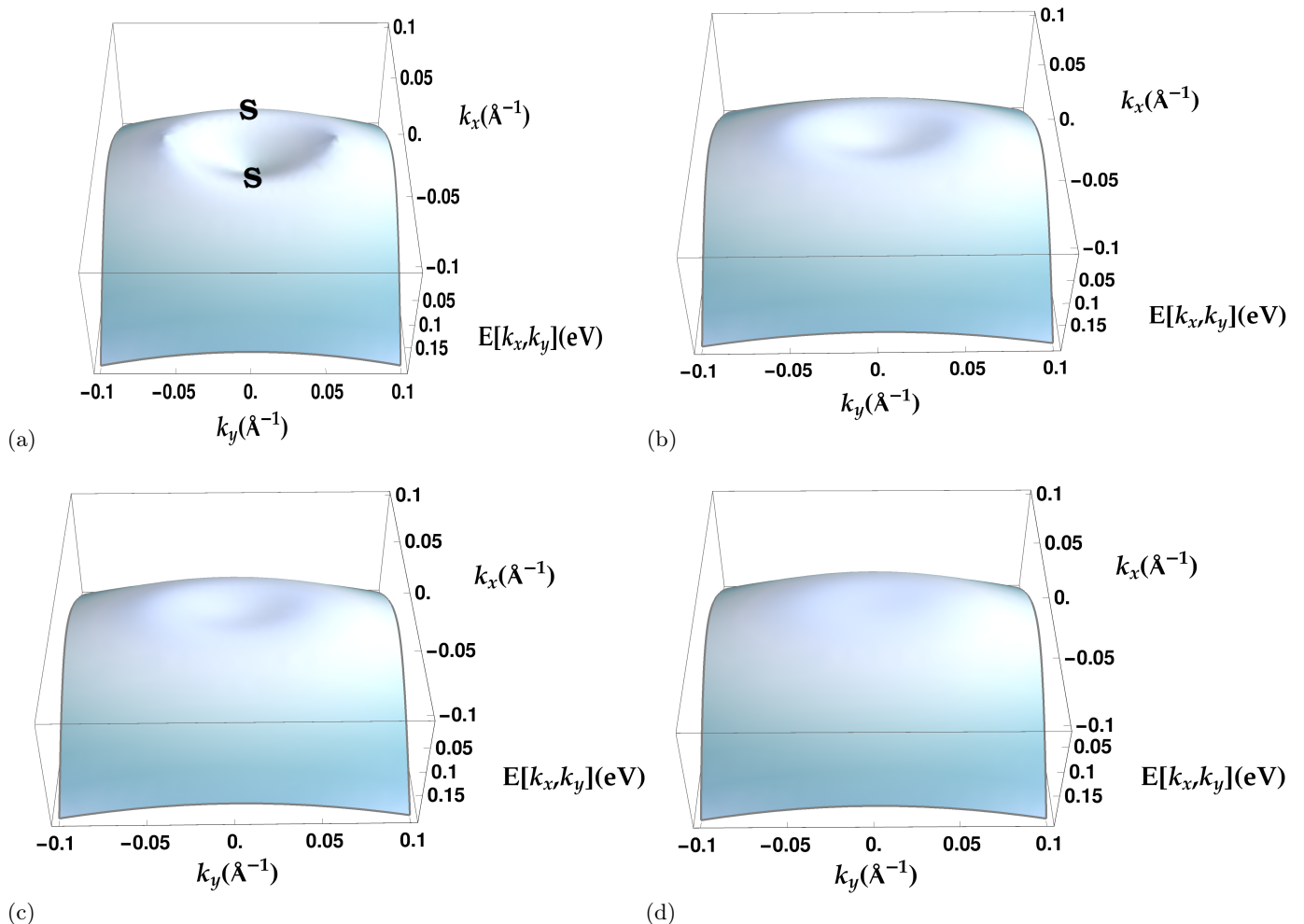


Figure 1. The two-dimensional Van-Hove singularities on the TCI surface (indicated by 'S') for (a)  $M = 0.0$ , (b)  $M = 0.04$ , (c)  $M = 0.05$ , and (d)  $M = 0.07$  (in eV) where  $v_x = 2.4 \text{ eV } \text{\AA}^{-1}$ ,  $v_y = 1.3 \text{ eV } \text{\AA}^{-1}$ ,  $m = 0.07 \text{ eV}$  and  $\delta = 0.026 \text{ eV}$  (values taken from [6]). We find that beyond  $M \approx 0.05 \text{ eV}$ , there are no Van-Hove singularities in the surface electronic spectrum.

to the Van Hove singularities. Here  $h_4$  refers to scattering processes between different valleys within a band  $i$ . The couplings  $h_1$ ,  $h_2$  and  $h_3$  represent exchange effects, Coulomb interaction and pair hopping, respectively, between electrons in different bands. Due to the distinctive phase dependences of the form factors, the interactions which correspond to spin-antiparallel configurations have an additional phase dependence of  $\exp[i(\theta_k - \theta_{k'})]$  and transform as  $\ell = 1$  functions in 2D, while those corresponding to spin-parallel configurations transform as  $\ell = 0$  functions. This implies that Coulomb interactions between the surface electrons generally depend on their relative spin configuration, and we therefore distinguish between interactions between electrons with parallel and anti-parallel spin configurations in our analysis. In the absence of a spin-splitting term in the Hamiltonian, the momentum-dependence of the interactions can be incorporated entirely into the aforementioned phase

factors. In our earlier analysis in [22], we have neglected the momentum-dependence of the absolute values of the form factors  $u_{\uparrow, \downarrow}$  (for each of the valleys). However, in the presence of a spin-splitting term  $M$ , the degeneracy between spins  $\uparrow$  and  $\downarrow$  is broken, and the complex form factors  $u_{\uparrow}$  and  $u_{\downarrow}$  differ both in amplitude and phase.

### 3. RENORMALIZATION GROUP EQUATIONS IN THE PRESENCE OF SPIN-SPLITTING

We perform our RG analysis with Fermi patches located at the two points  $X_1$  and  $X_2$  on the (001) surface, near the Van Hove singularities. As mentioned earlier, the phases arising from the form factors distinguish between electron interactions with parallel and antiparallel spin configurations, and so each of the couplings  $h_i$  (for the scattering channel  $i = 1 - 4$ ) in our RG analysis now have two components  $h_i^{\sigma\sigma}$  and  $h_i^{\sigma\bar{\sigma}}$ , which we

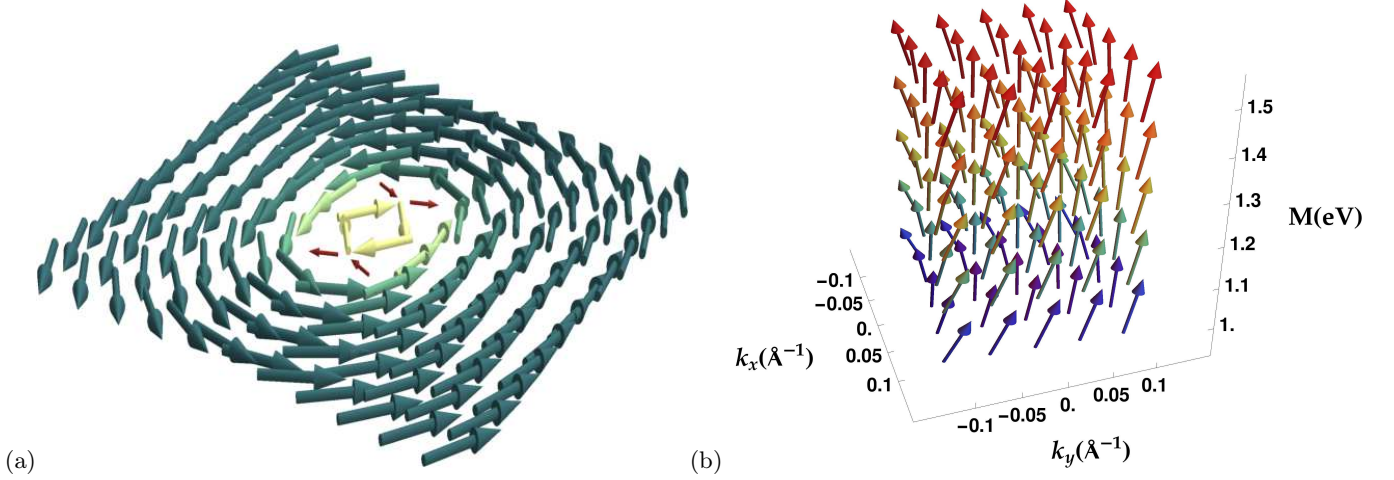


Figure 2. The spin texture  $\langle \vec{s}(k_x, k_y) \rangle = (\langle s_x \rangle, \langle s_y \rangle, \langle s_z \rangle)$  on the TCI surface (where  $k_x$  and  $k_y$  are measured in  $\text{\AA}^{-1}$ ) for the band with a positive energy lying closest to the Fermi level, with (a)  $M = 0.0$  eV, and (b)  $M$  in the range 1 to 1.5 eV. When  $M$  is small, the TCI surface continues to have a chiral spin texture, shown in (a), and for larger values of  $M$ , the spins gradually develop an out-of-plane polarization.

shall denote as  $h_i^0$  (for  $\ell = 0$ ) and  $h_i^1$  (for  $\ell = 1$ ) respectively. Moreover, the two spin components  $\uparrow$  and  $\downarrow$  are inequivalent in the presence of the Zeeman splitting term, and this gives rise to additional components for the couplings. To simplify our analysis, we have integrated out the momentum-dependence of the absolute values of the form factors  $|u_\uparrow(\vec{k}, M)|^2$  and  $|u_\downarrow(\vec{k}, M)|^2$  for the two spin components, over a suitable range of two-dimensional momenta  $(k_x, k_y)$  around the  $\bar{X}$  points (chosen to be  $0.1 \text{\AA}^{-1}$  for our calculations, based on the scale associated with the dispersion in momentum space as shown in Fig. 1), and normalized the results with respect to  $|u_\uparrow(\vec{k}, 0)|^2$  and  $|u_\downarrow(\vec{k}, 0)|^2$  respectively. Henceforth, we shall denote these  $k$ -integrated form factors by  $v_\uparrow$  and  $v_\downarrow$  for simplicity. The couplings constants  $h_i$  associated with the RG flows either involve two factors of either  $v_\uparrow$  or  $v_\downarrow$ , or one factor of each. Clearly, for  $M > 0$ , we have  $v_\uparrow(M) > 1$  and  $v_\downarrow(M) < 1$  for the positive energy eigenstates, and the ratio  $\frac{v_\uparrow(M)}{v_\downarrow(M)}$  increases with an increase in  $M$ . Corresponding to every scattering channel  $h_i$ , we then have four components  $h_i^{\uparrow\uparrow}$ ,  $h_i^{\downarrow\downarrow}$ ,  $h_i^{\uparrow\downarrow}$  and  $h_i^{\downarrow\uparrow}$ , alternately denoted by  $h_i^0$ ,  $h_i^2$ ,  $h_i^1$  and  $h_i^3$  respectively. This gives us a set of 16 coupling constants. The different coupling constants for interactions within a patch as well as between patches are shown in Fig. 3, taking into account the explicit factors of  $v_\uparrow$  and  $v_\downarrow$ . For  $M \gtrsim 0.05$  eV, one also has to take into account the absence of the Van-Hove singularities in the spectrum. We have performed calculations for higher values of magnetization as well, and found that the qualitative behavior of the system in that regime is very similar to what we discuss below. Therefore, we confine our attention to situations where Van-Hove singularities are present, since that gives us

high transition temperatures even in the weak-coupling regime.

We perform RG analysis up to one-loop level, integrating out high-energy degrees of freedom gradually from an energy cutoff  $\Lambda$ , which is the bandwidth. The susceptibilities in the different channels schematically behave as  $\chi_0^{pp}(\omega) \sim \ln[\Lambda/\omega] \ln[\Lambda/\max(\omega, \mu)]$ ,  $\chi_Q^{ph}(\omega) \sim \ln[\Lambda/\max(\omega, \mu)] \ln[\Lambda/\max(\omega, t)]$  and  $\chi_0^{ph}(\omega), \chi_Q^{pp}(\omega) \sim \ln[\Lambda/\max(\omega, \mu)]$ , where  $\omega$  denotes the energy away from the Van Hove singularities and  $t$  represents terms in the Hamiltonian that destroy the perfect nesting. In what follows, we shall use  $y \equiv \ln^2[\Lambda/\omega] \sim \chi_0^{pp}$  as the RG flow parameter, and describe the relative weight of the other channels as  $d_1(y) = \frac{d\chi_Q^{ph}}{dy}$ ,  $d_2(y) = \frac{d\chi_0^{ph}}{dy}$  and  $d_3(y) = -\frac{d\chi_Q^{pp}}{dy}$ . The factor  $d_1(y)$ , which incorporates the effects of imperfect nesting, is taken to be a function  $\frac{1}{\sqrt{1+y}}$  [19], interpolating smoothly in between the limits  $d_1(y=0) = 1$  and  $d_1(y \gg 1) = \frac{1}{\sqrt{y}}$ . We also assume that  $d_2, d_3 \ll d_1$ , and neglect the terms in the RG equations with these coefficients. The RG equations are obtained by evaluating second-order diagrams and collecting the respective combinatoric prefactors, for each of the interactions  $h_1, h_2, h_3$  and  $h_4$ . The diagrams for the coupling  $h_2$  are pictorially illustrated in [22]. The final set of RG equations obtained by taking into account the multiplicative factors  $v_\sigma$  and  $v_{\bar{\sigma}}$ , are given by

$$\begin{aligned} \frac{dh_1^{\sigma\sigma}}{dy} = & \frac{2}{\sqrt{1+y}} ((h_3^{\sigma\sigma})^2 v_\sigma^2 \\ & - (h_1^{\sigma\sigma})^2 v_\sigma^2 - (h_3^{\sigma\bar{\sigma}})(h_3^{\bar{\sigma}\sigma}) v_\sigma^2 \\ & - (h_1^{\sigma\bar{\sigma}})(h_1^{\bar{\sigma}\sigma}) v_\sigma^2 + 2(h_1^{\sigma\sigma})(h_2^{\sigma\sigma}) v_\sigma^2) \end{aligned} \quad (3)$$

$$\begin{aligned} \frac{dh_1^{\bar{\sigma}\sigma}}{dy} &= \frac{2}{\sqrt{1+y}} ((h_3^{\bar{\sigma}\sigma})^2 v_\sigma^2 \\ &\quad - (h_1^{\bar{\sigma}\sigma})^2 v_\sigma^2 - (h_3^{\bar{\sigma}\sigma})(h_3^{\sigma\bar{\sigma}}) v_\sigma^2 \\ &\quad - (h_1^{\bar{\sigma}\sigma})(h_1^{\sigma\bar{\sigma}}) v_\sigma^2 + 2(h_1^{\bar{\sigma}\sigma})(h_2^{\bar{\sigma}\sigma}) v_\sigma^2) \end{aligned} \quad (4)$$

$$\begin{aligned} \frac{dh_1^{\sigma\bar{\sigma}}}{dy} &= \frac{2h_1^{\sigma\bar{\sigma}}}{\sqrt{1+y}} (- (h_1^{\bar{\sigma}\sigma}) v_\sigma^2 - (h_1^{\sigma\sigma}) v_\sigma^2 \\ &\quad + (h_2^{\sigma\sigma}) v_\sigma^2 + (h_2^{\bar{\sigma}\sigma}) v_\sigma^2) \end{aligned} \quad (5)$$

$$\begin{aligned} \frac{dh_1^{\bar{\sigma}\sigma}}{dy} &= \frac{2h_1^{\bar{\sigma}\sigma}}{\sqrt{1+y}} (- (h_1^{\bar{\sigma}\sigma}) v_\sigma^2 - (h_1^{\sigma\sigma}) v_\sigma^2 \\ &\quad + (h_2^{\sigma\sigma}) v_\sigma^2 + (h_2^{\bar{\sigma}\sigma}) v_\sigma^2) \end{aligned} \quad (6)$$

$$\frac{dh_2^{\sigma\sigma}}{dy} = \frac{2}{\sqrt{1+y}} ((h_2^{\sigma\sigma})^2 + (h_3^{\sigma\sigma})^2) v_\sigma^2 \quad (7)$$

$$\frac{dh_2^{\bar{\sigma}\sigma}}{dy} = \frac{2}{\sqrt{1+y}} ((h_2^{\bar{\sigma}\sigma})^2 + (h_3^{\bar{\sigma}\sigma})^2) v_\sigma^2 \quad (8)$$

$$\frac{dh_2^{\sigma\bar{\sigma}}}{dy} = \frac{2}{\sqrt{1+y}} ((h_2^{\sigma\bar{\sigma}})^2 + (h_3^{\sigma\bar{\sigma}})^2) v_\sigma v_{\bar{\sigma}} \quad (9)$$

$$\frac{dh_2^{\bar{\sigma}\sigma}}{dy} = \frac{2}{\sqrt{1+y}} ((h_2^{\bar{\sigma}\sigma})^2 + (h_3^{\bar{\sigma}\sigma})^2) v_\sigma v_{\bar{\sigma}} \quad (10)$$

$$\begin{aligned} \frac{dh_3^{\sigma\sigma}}{dy} &= -4h_3^{\sigma\sigma} h_4^{\sigma\sigma} v_\sigma^2 + \frac{2}{\sqrt{1+y}} (4h_2^{\sigma\sigma} h_3^{\sigma\sigma} v_\sigma^2 \\ &\quad - h_1^{\bar{\sigma}\sigma} h_3^{\sigma\bar{\sigma}} v_\sigma^2 - h_1^{\sigma\bar{\sigma}} h_3^{\bar{\sigma}\sigma} v_\sigma^2) \end{aligned} \quad (11)$$

$$\begin{aligned} \frac{dh_3^{\bar{\sigma}\sigma}}{dy} &= -4h_3^{\bar{\sigma}\sigma} h_4^{\bar{\sigma}\sigma} v_\sigma^2 + \frac{2}{\sqrt{1+y}} (4h_2^{\bar{\sigma}\sigma} h_3^{\bar{\sigma}\sigma} v_\sigma^2 \\ &\quad - h_1^{\bar{\sigma}\sigma} h_3^{\sigma\bar{\sigma}} v_\sigma^2 - h_1^{\sigma\bar{\sigma}} h_3^{\bar{\sigma}\sigma} v_\sigma^2) \end{aligned} \quad (12)$$

$$\begin{aligned} \frac{dh_3^{\sigma\bar{\sigma}}}{dy} &= -4h_3^{\sigma\bar{\sigma}} h_4^{\sigma\bar{\sigma}} v_\sigma v_{\bar{\sigma}} \\ &\quad + \frac{2}{\sqrt{1+y}} (2h_2^{\sigma\bar{\sigma}} h_3^{\sigma\bar{\sigma}} v_\sigma v_{\bar{\sigma}} + \\ &\quad h_3^{\sigma\bar{\sigma}} (h_2^{\sigma\sigma} v_\sigma^2 + h_2^{\bar{\sigma}\sigma} v_\sigma^2 - h_1^{\sigma\sigma} v_\sigma^2 - h_1^{\bar{\sigma}\sigma} v_\sigma^2)) \end{aligned} \quad (13)$$

$$\begin{aligned} \frac{dh_3^{\bar{\sigma}\sigma}}{dy} &= -4h_3^{\bar{\sigma}\sigma} h_4^{\bar{\sigma}\sigma} v_\sigma v_{\bar{\sigma}} \\ &\quad + \frac{2}{\sqrt{1+y}} (2h_2^{\bar{\sigma}\sigma} h_3^{\bar{\sigma}\sigma} v_\sigma v_{\bar{\sigma}} + \\ &\quad h_3^{\bar{\sigma}\sigma} (h_2^{\sigma\sigma} v_\sigma^2 + h_2^{\bar{\sigma}\sigma} v_\sigma^2 - h_1^{\sigma\sigma} v_\sigma^2 - h_1^{\bar{\sigma}\sigma} v_\sigma^2)) \end{aligned} \quad (14)$$

$$\frac{dh_4^{\sigma\sigma}}{dy} = -2((h_3^{\sigma\sigma})^2 + (h_4^{\sigma\sigma})^2) v_\sigma^2 \quad (15)$$

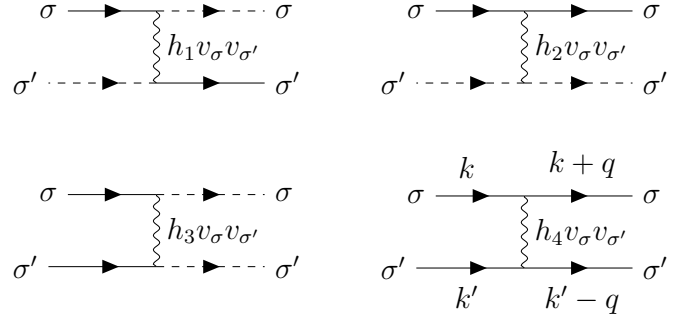


Figure 3. Couplings  $h_i$  defined on a patch ( $h_4$ ) and between the two patches ( $h_1, h_2, h_3$ ). There is a momentum-dependence associated with all of these couplings. Each of the possible scattering processes within a patch are denoted by  $h_4$  in our analysis. The spin labels  $\sigma, \sigma'$  correspond to specific spin components of the spinor wavefunctions associated with the different bands under consideration. The nature of the couplings considered here are very similar to those defined in [22], except now each of them also has an explicit factor  $v_\sigma v_{\sigma'}$  depending on the particular spin combination being considered.

$$\frac{dh_4^{\bar{\sigma}\sigma}}{dy} = -2((h_3^{\bar{\sigma}\sigma})^2 + (h_4^{\bar{\sigma}\sigma})^2) v_\sigma^2 \quad (16)$$

$$\frac{dh_4^{\sigma\bar{\sigma}}}{dy} = -2((h_3^{\sigma\bar{\sigma}})^2 + (h_4^{\sigma\bar{\sigma}})^2) v_\sigma v_{\bar{\sigma}} \quad (17)$$

$$\frac{dh_4^{\bar{\sigma}\sigma}}{dy} = -2((h_3^{\bar{\sigma}\sigma})^2 + (h_4^{\bar{\sigma}\sigma})^2) v_\sigma v_{\bar{\sigma}} \quad (18)$$

where the factors of 2 on the right hand side of each equation are due to equal contributions from the two valleys corresponding to every patch.

#### 4. SUSCEPTIBILITIES

In order to investigate the possible electronic instabilities in this system, we shall now evaluate the susceptibilities  $\chi$  for various types of order, by introducing infinitesimal test vertices corresponding to different kinds of pairing into the action, such as  $\Delta_a \psi_{a\sigma}^\dagger \psi_{a\sigma'}^\dagger + \Delta_a^* \psi_{a\sigma} \psi_{a\sigma'}$  for the patch  $a = 1, 2$  (where the spin labels  $\sigma, \sigma'$  on the fermions denote the presence or absence of the phase factors  $\exp[i\theta_k]$ ) corresponding to particle-particle pairing on a patch [19, 22].

The renormalization of the test vertex corresponding to particle-particle pairing on a patch is governed by the equation

$$\frac{\partial}{\partial y} \begin{pmatrix} \Delta_1 \\ \Delta_2 \end{pmatrix} = 2v_\sigma v_{\bar{\sigma}} \begin{pmatrix} h_4^{\sigma\bar{\sigma}} & h_3^{\sigma\bar{\sigma}} \\ h_3^{\bar{\sigma}\sigma} & h_4^{\bar{\sigma}\sigma} \end{pmatrix} \begin{pmatrix} \Delta_1 \\ \Delta_2 \end{pmatrix} \quad (19)$$

since we can only consider Cooper pairing in the  $p$ -wave channel for effectively spinless electrons on the TCI surface, where  $\sigma, \bar{\sigma} = \uparrow, \downarrow$  in this case. By transforming to

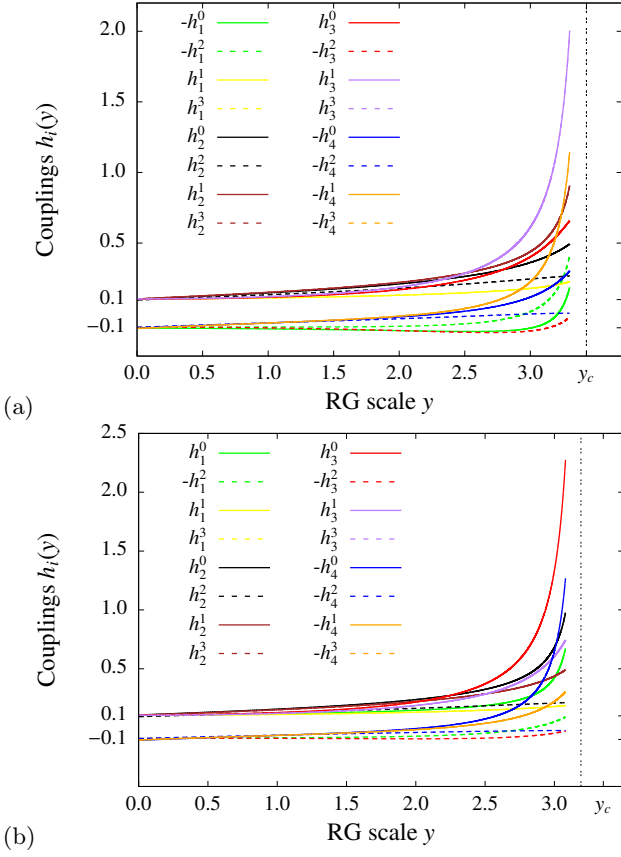


Figure 4. The RG flows for (a)  $M = 4$  meV and (b)  $M = 9$  meV where the critical value of spin-splitting  $M_c \approx 6.1$  meV. The fixed point value  $y_c \approx 3.43$  for (a) and  $y_c \approx 3.2$  for (b) above. Here, the initial values for each of the dimensionless couplings is taken to be 0.1, and a Hund's splitting of 5% ( $\frac{|h_i^{\sigma\bar{\sigma}} - h_i^{\sigma\sigma}|}{|h_i^{\sigma\bar{\sigma}}|} = 0.05$ ) is introduced initially such that  $h_i^{\sigma\bar{\sigma}} > h_i^{\sigma\sigma}$  for  $i = 1 - 4$  and  $\sigma = \uparrow, \downarrow$ . Clearly, the leading couplings near the instability threshold correspond to spin-antiparallel configurations for  $M < M_c$ , while the spin  $\uparrow$  component of each of the couplings dominates for  $M > M_c$ . Here the couplings  $h_i^{\uparrow\uparrow}, h_i^{\downarrow\downarrow}, h_i^{\uparrow\downarrow}$  and  $h_i^{\downarrow\uparrow}$  are denoted respectively by  $h_i^0, h_i^2, h_i^1$  and  $h_i^3$ , for clarity. The factors of  $v_\uparrow$  and  $v_\downarrow$  have been absorbed into the couplings constants  $h_i^\ell$  ( $\ell = 0 - 3$ ) in the above plots, for simplicity in notation.

the eigenvector basis, we can obtain different possible order parameters, and choose the one corresponding to the most negative eigenvalue. The vertices with positive eigenvalues are suppressed under RG flow. The renormalization equations for the test vertices for other kinds of pairing can be similarly obtained. The diagrams corresponding to the renormalization of the different pairing vertices considered by us are shown in [22], and we consider similar kinds of pairing here, although the total number of instabilities possible increases in this case due to the lifting of spin degeneracy by the Zeeman splitting term in the Hamiltonian.

Each of the couplings has an asymptotic form  $h_i(y) =$

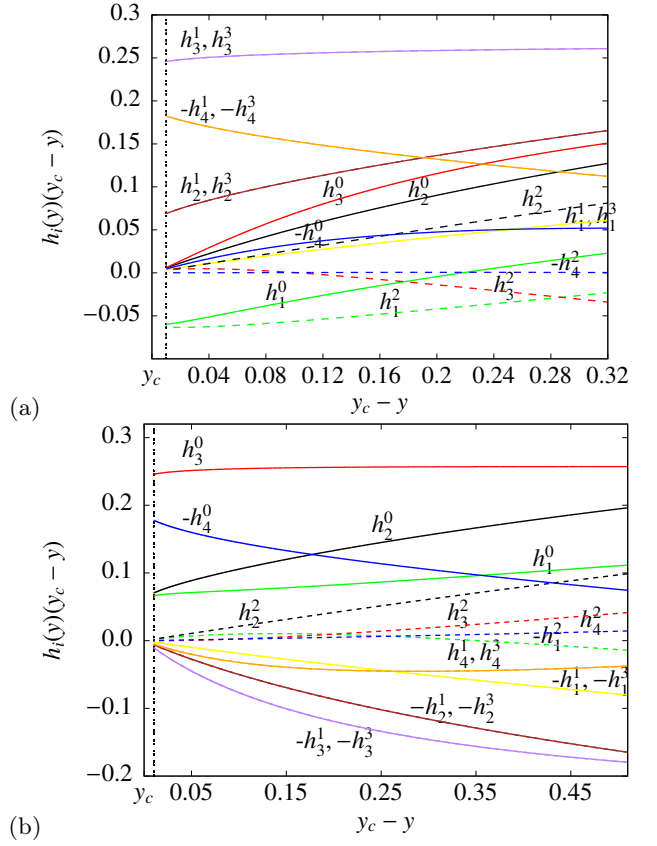


Figure 5. The order of the fixed-point values for the different couplings  $h_i^\ell$  ( $\ell = 0 - 3$ ) at the critical point  $y_c$  for (a)  $M = 4$  meV and (b)  $M = 9$  meV, where the critical spin-splitting  $M_c \approx 6.1$  meV. Here, the initial values for each of the dimensionless couplings is taken to be 0.1, and a Hund's splitting of 5% ( $\frac{|h_i^{\sigma\bar{\sigma}} - h_i^{\sigma\sigma}|}{|h_i^{\sigma\bar{\sigma}}|} = 0.05$ ) is introduced initially such that  $h_i^{\sigma\bar{\sigma}} > h_i^{\sigma\sigma}$  for  $i = 1 - 4$  and  $\sigma = \uparrow, \downarrow$ . The above plots show the evolution of  $h_i^\ell(y)$  as a function of  $(y_c - y)$  close to the fixed point  $y_c$ , where each coupling constant  $h_i^\ell$  has an asymptotic form  $\frac{g_i^\ell}{y_c - y}$ , and the  $y$ -intercepts of curves shown give an estimate of the fixed-point values  $g_i^\ell$  for the different couplings. This clearly indicates that the leading couplings for  $M < M_c$  correspond to the  $\ell = 1$  and  $\ell = 3$  channels, for spin-antiparallel configurations, in the presence of a finite Hund's splitting, while for  $M > M_c$  these correspond to the spin  $\uparrow$  ( $\ell = 0$ ) channel. As in Fig.4, the factors of  $v_\uparrow$  and  $v_\downarrow$  corresponding to each coupling have been absorbed into  $h_i^\ell$  ( $\ell = 0 - 3$ ).

$\frac{g_i^{\sigma\sigma'}}{y_c - y}$  [18, 19] at the threshold. At an electronic instability, the most divergent susceptibility  $\chi$  determines the nature of the ordered phase. The exponents  $\alpha$  for susceptibilities  $\chi$  corresponding to the various order parameters (which have a general form  $\chi \propto (y_c - y)^\alpha$ ) are functions of the fixed point values of the couplings  $g_i^{\sigma\sigma'}$ . The channel where the instability is most likely to take place has the most singular susceptibility, i.e. the most negative value of  $\alpha$ . By substituting the asymptotic form for the couplings  $h_i^{\sigma\sigma'}$  into the above eq.19 and



the corresponding equations for other kinds of pairing, we have obtained the exponents  $\alpha$  for intrapatch  $p$ -wave pairing, charge-density wave, spin-density wave, uniform spin, charge compressibility ( $\kappa$ ) and finite-momentum  $\pi$  pairing, which are given as follows-

$$\begin{aligned}
\alpha_{pwave} &= 2(g_4^{\sigma\bar{\sigma}} - g_3^{\sigma\bar{\sigma}})v_\sigma v_{\bar{\sigma}} \\
\alpha_\kappa &= (g_1^{\sigma\sigma}(v_\sigma)^2 + g_4^{\sigma\bar{\sigma}}(v_\sigma v_{\bar{\sigma}}) - g_2^{\sigma\sigma}(v_\sigma)^2 \\
&\quad - g_2^{\sigma\bar{\sigma}}(v_\sigma v_{\bar{\sigma}}))d_2(y_c) \\
\alpha_s &= -(g_4^{\sigma\bar{\sigma}} + g_1^{\sigma\bar{\sigma}})(v_\sigma v_{\bar{\sigma}})d_2(y_c) \\
\alpha_\pi^{\sigma\bar{\sigma}} &= (g_1^{\sigma\bar{\sigma}} + g_2^{\sigma\bar{\sigma}})(v_\sigma v_{\bar{\sigma}})d_3(y_c) \\
\alpha_\pi^{\sigma\sigma} &= (v_\sigma)^2(g_1^{\sigma\sigma} + g_2^{\sigma\sigma})d_3(y_c) \\
\alpha_{CDW} &= (g_1^{\sigma\sigma}(v_\sigma)^2 - g_3^{\sigma\bar{\sigma}}(v_\sigma v_{\bar{\sigma}}) + g_1^{\sigma\bar{\sigma}}(v_\sigma v_{\bar{\sigma}}) \\
&\quad - g_2^{\sigma\sigma}(v_\sigma)^2)d_1(y_c) \\
\alpha_{SDW} &= -2(g_3^{\sigma\bar{\sigma}} + g_2^{\sigma\bar{\sigma}})(v_\sigma v_{\bar{\sigma}})d_1(y_c) \quad (20)
\end{aligned}$$

The above expressions correspond to various spin combinations  $\sigma, \bar{\sigma} = \uparrow, \downarrow$ .

## 5. LADDER RG EQUATIONS IN THE ABSENCE OF HUND'S SPLITTING OF INTERACTIONS

Let us first consider a situation where the various components of interactions  $h_i$  in the different scattering channels  $i = 1 - 4$  are taken to be identical initially, with no Hund's splitting present. In this case, we find that even for a very small value of Zeeman splitting  $M$ , the leading components of the different kinds of interactions near the fixed point  $y_c$  correspond to spin  $\uparrow$  (i.e. the  $\ell = 0$  channel). Now, if we introduce test vertices for different kinds of pairing and calculate the exponents for the divergence of the respective susceptibilities, we find that each of the exponents  $\alpha$  is either positive or numerically close to zero. This indicates the absence of any electronic instabilities in this case. Clearly,  $p$ -wave superconductivity cannot be stabilized at energies corresponding to the fixed point of the parquet RG. However, when the Fermi energy  $E_F$  associated with the system exceeds the energy  $\omega_c$  corresponding to the critical point  $y_c$ , the RG flow must be terminated at  $E_F$ , and any possible instabilities will then depend on the order of the different couplings at the Fermi energy. These are determined using a ladder RG approach, which is described in [28].

Two kinds of vertices continue to flow logarithmically at energies below the Fermi energy  $E_F$ : vertices with

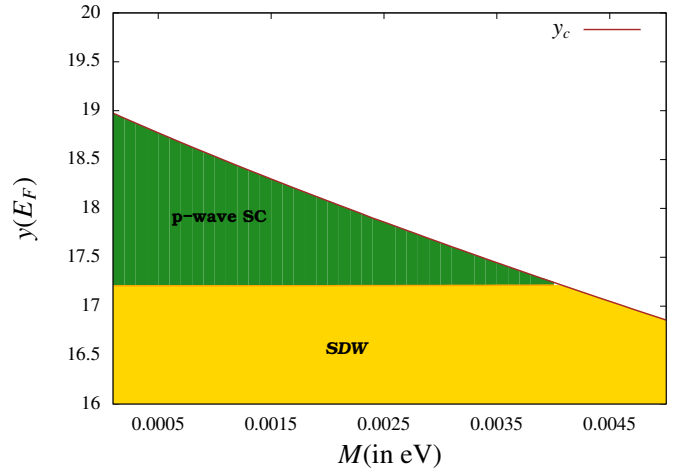


Figure 6. The phase diagram for  $y(E_F)$  as a function of the spin-splitting  $M$  when the initial value of each of the dimensionless RG couplings is chosen to be equal to 0.03. This shows that for large electron densities, it is possible to stabilize  $p$ -wave superconductivity for a range of values of the Fermi energy  $E_F$ , up till  $M \sim 4$  meV (in this case). The values on the  $y$ -axis as well as the value of  $M$  up to which  $p$ -wave superconductivity may be stabilized depend on the initial interaction strength. The latter decreases with an increase in the strength of electronic interactions.

zero total momentum, and with total momentum exactly equal to the nesting vector  $Q$  in two dimensions. The vertices with zero total momentum are the  $h_3$  and  $h_4$  terms in our RG analysis and the vertices with total momentum  $Q$  are the  $h_1$ ,  $h_2$  and  $h_3$  terms. The values of  $h_i$  at  $E_F$  act as the bare couplings for the theory at  $E < E_F$ . There are two kinds of  $h_3$  vertices with a momentum transfer  $Q$ ,  $h_{3a}$  and  $h_{3b}$  (for a detailed discussion, please refer to [28]) and we denote the  $h_3$  vertex with zero total momentum as  $h_{3c}$ . Following [28], we shall refer to the vertices with zero total momentum as  $h_i(0)$  and the vertices with total momentum  $Q$  as  $h_i(Q)$ . The ladder RG equations are obtained by considering those diagrams which still yield a logarithmic divergence [28].

The ladder RG equations for our system, where now  $y \equiv \ln[\frac{E_F}{\omega}]$ , are given as follows-

$$\begin{aligned}
\frac{dh_1^{\sigma\sigma}(Q)}{dy} &= 2((2(h_{3a}^{\sigma\sigma}(Q)h_{3b}^{\sigma\sigma}(Q) - (h_{3a}^{\sigma\sigma}(Q))^2)v_\sigma^2 \\
&\quad - (h_1^{\sigma\sigma}(Q))^2v_\sigma^2 - (h_{3a}^{\sigma\bar{\sigma}}(Q))(h_{3a}^{\bar{\sigma}\sigma}(Q))v_\sigma^2 - \\
&\quad (h_1^{\sigma\bar{\sigma}}(Q))(h_1^{\bar{\sigma}\sigma}(Q))v_\sigma^2 + 2(h_1^{\sigma\sigma}(Q))(h_2^{\sigma\sigma}(Q))v_\sigma^2) \\
\frac{dh_1^{\bar{\sigma}\bar{\sigma}}(Q)}{dy} &= 2((2(h_{3a}^{\bar{\sigma}\bar{\sigma}}(Q))(h_{3b}^{\bar{\sigma}\bar{\sigma}}(Q)) - (h_{3a}^{\bar{\sigma}\bar{\sigma}}(Q))^2)v_\sigma^2 \\
&\quad - (h_1^{\bar{\sigma}\bar{\sigma}}(Q))^2v_\sigma^2 - (h_{3a}^{\bar{\sigma}\sigma}(Q))(h_{3a}^{\sigma\bar{\sigma}}(Q))v_\sigma^2 - \\
&\quad (h_1^{\bar{\sigma}\sigma}(Q))(h_1^{\sigma\bar{\sigma}}(Q))v_\sigma^2 + \\
&\quad 2(h_1^{\bar{\sigma}\bar{\sigma}}(Q))(h_2^{\bar{\sigma}\bar{\sigma}}(Q))v_\sigma^2)
\end{aligned}$$

$$\begin{aligned} \frac{dh_1^{\sigma\bar{\sigma}}(Q)}{dy} &= 2(h_{3a}^{\sigma\bar{\sigma}}(Q)(h_{3b}^{\sigma\bar{\sigma}}(Q) - h_{3a}^{\sigma\bar{\sigma}}(Q))v_\sigma^2 \\ &\quad + h_{3a}^{\sigma\bar{\sigma}}(Q)(h_{3b}^{\sigma\sigma}(Q) - h_{3a}^{\sigma\sigma}(Q))v_\sigma^2 + h_1^{\sigma\bar{\sigma}}(Q) \\ &\quad (- (h_1^{\sigma\bar{\sigma}}(Q))v_\sigma^2 - (h_1^{\sigma\sigma}(Q))v_\sigma^2 + (h_2^{\sigma\sigma}(Q))v_\sigma^2 \\ &\quad + (h_2^{\sigma\bar{\sigma}}(Q))v_\sigma^2)) \end{aligned}$$

$$\begin{aligned} \frac{dh_1^{\bar{\sigma}\sigma}(Q)}{dy} &= 2(h_{3a}^{\bar{\sigma}\sigma}(Q)(h_{3b}^{\bar{\sigma}\sigma}(Q) - h_{3a}^{\bar{\sigma}\sigma}(Q))v_\sigma^2 \\ &\quad + h_{3a}^{\bar{\sigma}\sigma}(Q)(h_{3b}^{\sigma\sigma}(Q) - h_{3a}^{\sigma\sigma}(Q))v_\sigma^2 + h_1^{\bar{\sigma}\sigma}(Q) \\ &\quad (- (h_1^{\bar{\sigma}\sigma}(Q))v_\sigma^2 - (h_1^{\sigma\sigma}(Q))v_\sigma^2 + (h_2^{\sigma\sigma}(Q))v_\sigma^2 \\ &\quad + (h_2^{\sigma\bar{\sigma}}(Q))v_\sigma^2)) \end{aligned}$$

$$\frac{dh_2^{\sigma\sigma}(Q)}{dy} = 2((h_2^{\sigma\sigma}(Q))^2 + (h_{3b}^{\sigma\sigma}(Q))^2)v_\sigma^2$$

$$\frac{dh_2^{\bar{\sigma}\bar{\sigma}}(Q)}{dy} = 2((h_2^{\bar{\sigma}\bar{\sigma}}(Q))^2 + (h_{3b}^{\bar{\sigma}\bar{\sigma}}(Q))^2)v_\sigma^2$$

$$\frac{dh_2^{\sigma\bar{\sigma}}(Q)}{dy} = 2((h_2^{\sigma\bar{\sigma}}(Q))^2 + (h_{3b}^{\sigma\bar{\sigma}}(Q))^2)v_\sigma v_\sigma$$

$$\frac{dh_2^{\bar{\sigma}\sigma}(Q)}{dy} = 2((h_2^{\bar{\sigma}\sigma}(Q))^2 + (h_{3b}^{\bar{\sigma}\sigma}(Q))^2)v_\sigma v_\sigma$$

$$\begin{aligned} \frac{dh_{3a}^{\sigma\sigma}(Q)}{dy} &= 2(2h_1^{\sigma\sigma}(Q)(h_{3b}^{\sigma\sigma}(Q) \\ &\quad - h_{3a}^{\sigma\sigma}(Q))v_\sigma^2 + 2h_2^{\sigma\sigma}(Q)h_{3a}^{\sigma\sigma}(Q)v_\sigma^2 \\ &\quad - h_1^{\bar{\sigma}\sigma}(Q)h_{3a}^{\sigma\bar{\sigma}}(Q)v_\sigma^2 - h_1^{\sigma\bar{\sigma}}(Q)h_{3a}^{\bar{\sigma}\sigma}(Q)v_\sigma^2) \end{aligned}$$

$$\frac{dh_{3b}^{\sigma\sigma}(Q)}{dy} = 4h_2^{\sigma\sigma}(Q)h_{3b}^{\sigma\sigma}(Q)v_\sigma^2$$

$$\frac{dh_{3c}^{\sigma\sigma}(0)}{dy} = -4h_4^{\sigma\sigma}(0)h_{3c}^{\sigma\sigma}(0)v_\sigma^2$$

$$\begin{aligned} \frac{dh_{3a}^{\bar{\sigma}\bar{\sigma}}(Q)}{dy} &= 2(2h_1^{\bar{\sigma}\bar{\sigma}}(Q)(h_{3b}^{\bar{\sigma}\bar{\sigma}}(Q) \\ &\quad - h_{3a}^{\bar{\sigma}\bar{\sigma}}(Q))v_\sigma^2 + 2h_2^{\bar{\sigma}\bar{\sigma}}(Q)h_{3a}^{\bar{\sigma}\bar{\sigma}}(Q)v_\sigma^2 \\ &\quad - h_1^{\sigma\bar{\sigma}}(Q)h_{3a}^{\bar{\sigma}\sigma}(Q)v_\sigma^2 - h_1^{\bar{\sigma}\sigma}(Q)h_{3a}^{\sigma\bar{\sigma}}(Q)v_\sigma^2) \end{aligned}$$

$$\frac{dh_{3b}^{\bar{\sigma}\bar{\sigma}}(Q)}{dy} = 4h_2^{\bar{\sigma}\bar{\sigma}}(Q)h_{3b}^{\bar{\sigma}\bar{\sigma}}(Q)v_\sigma^2$$

$$\frac{dh_{3c}^{\bar{\sigma}\bar{\sigma}}(0)}{dy} = -4h_4^{\bar{\sigma}\bar{\sigma}}(0)h_{3c}^{\bar{\sigma}\bar{\sigma}}(0)v_\sigma^2$$

$$\begin{aligned} \frac{dh_{3a}^{\sigma\bar{\sigma}}(Q)}{dy} &= 2(h_1^{\sigma\bar{\sigma}}(Q)(h_{3b}^{\sigma\sigma}(Q) - h_{3a}^{\sigma\sigma}(Q))v_\sigma^2 \\ &\quad + h_1^{\sigma\bar{\sigma}}(Q)(h_{3b}^{\bar{\sigma}\bar{\sigma}}(Q) - h_{3a}^{\bar{\sigma}\bar{\sigma}}(Q))v_\sigma^2 + \\ &\quad h_{3a}^{\sigma\bar{\sigma}}(Q)(h_2^{\sigma\sigma}(Q)v_\sigma^2 + h_2^{\bar{\sigma}\bar{\sigma}}(Q)v_\sigma^2 \\ &\quad - h_1^{\sigma\sigma}(Q)v_\sigma^2 - h_1^{\bar{\sigma}\bar{\sigma}}(Q)v_\sigma^2)) \end{aligned}$$

$$\frac{dh_{3b}^{\sigma\bar{\sigma}}(Q)}{dy} = 4h_2^{\sigma\bar{\sigma}}(Q)h_{3b}^{\sigma\bar{\sigma}}(Q)v_\sigma v_\sigma$$

$$\frac{dh_{3c}^{\sigma\bar{\sigma}}(0)}{dy} = -4h_4^{\sigma\bar{\sigma}}(0)h_{3c}^{\sigma\bar{\sigma}}(0)v_\sigma v_\sigma$$

$$\begin{aligned} \frac{dh_{3a}^{\bar{\sigma}\sigma}(Q)}{dy} &= 2(h_1^{\bar{\sigma}\sigma}(Q)(h_{3b}^{\sigma\sigma}(Q) - h_{3a}^{\sigma\sigma}(Q))v_\sigma^2 \\ &\quad + h_1^{\bar{\sigma}\sigma}(Q)(h_{3b}^{\bar{\sigma}\bar{\sigma}}(Q) - h_{3a}^{\bar{\sigma}\bar{\sigma}}(Q))v_\sigma^2 + \\ &\quad h_{3a}^{\bar{\sigma}\sigma}(Q)(h_2^{\sigma\sigma}(Q)v_\sigma^2 + h_2^{\bar{\sigma}\bar{\sigma}}(Q)v_\sigma^2 \\ &\quad - h_1^{\sigma\sigma}(Q)v_\sigma^2 - h_1^{\bar{\sigma}\bar{\sigma}}(Q)v_\sigma^2)) \end{aligned}$$

$$\frac{dh_{3b}^{\bar{\sigma}\sigma}(Q)}{dy} = 4h_2^{\bar{\sigma}\sigma}(Q)h_{3b}^{\bar{\sigma}\sigma}(Q)v_\sigma v_\sigma$$

$$\frac{dh_{3c}^{\bar{\sigma}\sigma}(0)}{dy} = -4h_4^{\bar{\sigma}\sigma}(0)h_{3c}^{\bar{\sigma}\sigma}(0)v_\sigma v_\sigma$$

$$\frac{dh_4^{\sigma\sigma}(0)}{dy} = -2((h_{3c}^{\sigma\sigma}(0))^2 + (h_4^{\sigma\sigma}(0))^2)v_\sigma^2$$

$$\frac{dh_4^{\bar{\sigma}\bar{\sigma}}(0)}{dy} = -2((h_{3c}^{\bar{\sigma}\bar{\sigma}}(0))^2 + (h_4^{\bar{\sigma}\bar{\sigma}}(0))^2)v_\sigma^2$$

$$\frac{dh_4^{\sigma\bar{\sigma}}(0)}{dy} = -2((h_{3c}^{\sigma\bar{\sigma}}(0))^2 + (h_4^{\sigma\bar{\sigma}}(0))^2)v_\sigma v_\sigma$$

$$\frac{dh_4^{\bar{\sigma}\sigma}(0)}{dy} = -2((h_{3c}^{\bar{\sigma}\sigma}(0))^2 + (h_4^{\bar{\sigma}\sigma}(0))^2)v_\sigma v_\sigma \quad (21)$$

From the above equations, we find

$$\frac{d(h_{3c}^{\sigma\bar{\sigma}}(0) - h_4^{\sigma\bar{\sigma}}(0))}{dy} = 2(h_{3c}^{\sigma\bar{\sigma}}(0) - h_4^{\sigma\bar{\sigma}}(0))^2 v_\sigma v_\sigma$$

for the superconducting vertex. These equations can be solved to give

$$h_3^{\sigma\bar{\sigma}}(0) - h_4^{\sigma\bar{\sigma}}(0) = \frac{(h_3^{\sigma\bar{\sigma}})_{E_F} - (h_4^{\sigma\bar{\sigma}})_{E_F}}{1 - 2v_\sigma v_\sigma ((h_3^{\sigma\bar{\sigma}})_{E_F} - (h_4^{\sigma\bar{\sigma}})_{E_F}) \log[\frac{E_F}{\omega}]}$$

A similar situation arises for the SDW instability in this regime. The competition between these instabilities depends on the respective energies at which different combinations of couplings diverge, and thus, on their values at



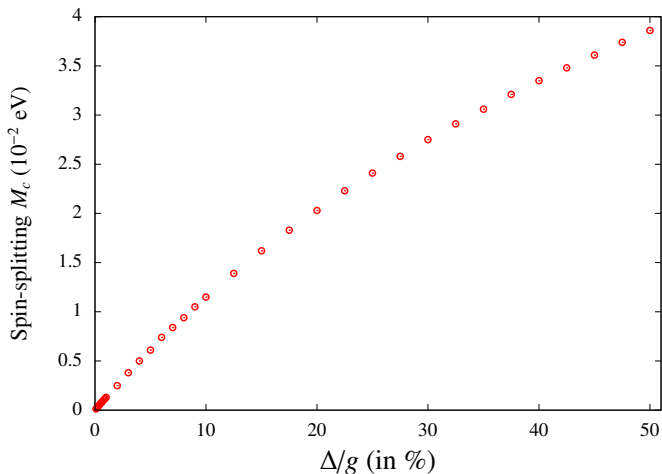


Figure 7. The behavior of the critical value of the spin-splitting  $M_c$  (in eV) as a function of the Hund's splitting  $\Delta$  as a percentage of the initial interaction  $g$  (i.e.  $h_i^{\sigma\sigma} = g$  initially for  $i = 1 - 4$  and  $\sigma = \uparrow, \downarrow$ ), where  $g = 0.1$  in this case. We find this behavior to be extremely insensitive to the initial value of interactions.

the Fermi energy  $E_F$ . The first instability occurs in the channel for which the coupling at  $\omega \sim E_F$  is the largest.

Thus, we find that for relatively large electron densities, when the Fermi energy  $E_F$  exceeds the energy ( $\omega_c$ ) corresponding to the critical point of the RG flow  $y_c$ , a  $p$ -wave superconducting order can be stabilized on the TCI surface up to a small value of the spin-splitting  $M$  ( $\sim 1$  meV). For larger values of Zeeman splitting introduced by an external magnetization, we find that a spin density wave (SDW) modulation may be possible over and above the expected uniform spin polarization on the surface, if the number density of electrons is sufficiently large. Although  $p$ -wave superconductivity is degraded even by a very small value of external magnetization in the absence of Hund's splitting, it is thus possible to stabilize this phase over a range of electron densities (and corresponding Fermi energies  $E_F$ ). A phase diagram for  $y(E_F)$  as a function of the spin-splitting term  $M$  is shown in Fig.6 for an initial value of 0.03 for each of the dimensionless couplings. It should be noted that the exact values on the  $y$ -axis, as well as the value of spin-splitting  $M$  (on the  $x$ -axis) beyond which  $p$ -wave superconductivity is no longer possible, is dependent on the initial interaction strength being considered. In particular, we find that the range of values of  $M$  for which  $p$ -wave superconductivity may be stabilized decreases with an increase in the strength of electronic interactions.

## 6. CRITICAL VALUES OF SPIN-SPLITTING FOR A FINITE HUND'S INTERACTION

For a multiorbital system like  $\text{Pb}_{1-x}\text{Sn}_x\text{Te}$ , one must also take into account the effects of Hund's splitting. This effect can be built into our RG analysis by assuming the initial values of interactions in each of the scattering channels  $i$  to be such that  $(h_i^{\sigma\bar{\sigma}} - h_i^{\sigma\sigma}) > 0$  (where  $\sigma = \uparrow, \downarrow$ ). In [22], we have shown that  $p$ -wave superconductivity is favored on the surface of  $\text{Pb}_{1-x}\text{Sn}_x\text{Te}$  even in the absence of Hund's splitting (i.e. when the interactions in the different channels are chosen to be identical initially). As seen in the previous section, in the presence of an external magnetization,  $p$ -wave superconductivity is destroyed (at the parquet level) even by a small value of Zeeman splitting. However, this is no longer true if a finite Hund's splitting is introduced initially. For a Hund's splitting of  $\Delta = h_i^{\sigma\bar{\sigma}} - h_i^{\sigma\sigma}$  (for each scattering channel  $i$ , where  $\sigma = \uparrow, \downarrow$ ),  $p$ -wave superconductivity continues to be the leading instability at the parquet level up to a finite value of the Zeeman splitting  $M$  (which depends on the value of  $\Delta$  being considered). Corresponding to each value of  $\Delta$ , a critical value of the spin-splitting  $M_c$  is obtained such that for  $M > M_c$ ,  $p$ -wave superconductivity is no longer possible. The variation of  $M_c$  as a function of the percentage Hund's splitting  $\frac{\Delta}{g}$  (where  $g$  denotes the initial value chosen for  $h_i^{\sigma\sigma}$  for  $i = 1 - 4$  with  $\sigma = \uparrow, \downarrow$ ) is shown in Fig.7 for  $g = 0.1$ . The behavior of  $M_c$  as a function of  $\frac{\Delta}{g}$  turns out to be remarkably insensitive to value of  $g$ , i.e. the initial interaction strength being considered (within the regime where perturbation theory is valid). To illustrate the nature of the most divergent couplings in the two limits, RG flows for  $M < M_c$  and  $M > M_c$  with a dimensionless initial repulsive interaction of 0.1 and a Hund's splitting of 5% ( $\frac{|h_i^{\sigma\bar{\sigma}} - h_i^{\sigma\sigma}|}{|h_i^{\sigma\sigma}|} = 0.05$ ) introduced initially, where the critical value of the Zeeman splitting  $M_c \approx 6.1$  meV, are shown in the Fig 4. The corresponding behavior of  $h_i^{\sigma\sigma'}(y)(y_c - y)$  as a function of  $(y_c - y)$ , which illustrates the order of the fixed point values  $g_i^{\sigma\sigma'}$  for the different couplings in the above-mentioned two cases, is shown in the Fig. 5.

## 7. SUMMARY AND DISCUSSION

In conclusion, we have studied the effect of an external magnetization on chiral  $p$ -wave superconductivity (predicted by us in [22]) on the (001) surface of the multi-orbital crystalline topological insulator  $\text{Pb}_{1-x}\text{Sn}_x\text{Te}$ , which was found to be sensitive to the sign of the Hund's splitting. We have shown that in the absence of Hund's splitting of interactions, the  $p$ -wave superconductivity may be destroyed even for very small values of the external magnetization. However, robust  $p$ -wave superconductivity, stable against moderately large values of the magneti-

zation is obtained upon introduction of a finite Hund's splitting of interactions, such that electrons with spin-antiparallel configurations interact more strongly than those with spin-parallel configurations.

It should be kept in mind that the conclusions drawn from the perturbative RG analysis are valid as long as the spin-splitting does not exceed the characteristic energy scale at the critical point. Otherwise, it would not be possible for interaction effects to dictate the ground state properties since their characteristic energies would then fall short of the spin-splitting scale.

While we have studied the effects of a time-reversal symmetry breaking perturbation on the surface superconductivity, further work is needed to understand the effects of disorder, which in other unconventional superconductors, is known to have a strong effect on their properties. Given that the superconductivity in our case arises from Berry phase effects, and not from Fermi surface deformations, we believe (see ref. [22] for a discussion) that moderate amounts of potential disorder will not cause destruction of the  $p$ -wave superconducting order [29, 30]. This is unlike the case of  $\text{Sr}_2\text{RuO}_4$ , where  $p$ -wave superconductivity is associated with Fermi surface deformations, and consequently, is very sensitive to potential disorder [31].

Recently, there have been reports of surface superconductivity induced on the surface of  $\text{Pb}_{0.6}\text{Sn}_{0.4}\text{Te}$  by forming a mesoscopic point contact using a nonsuperconducting metal [32], with a transition temperature in the range 3.7-6.5 K, although the symmetry of the superconducting order was not confirmed. Our predictions may be verified by examining the sensitivity of the superconducting order to magnetic doping on the (001) surface of the TCI.

Another interesting direction would be to further study the properties of the  $p$ -wave superconductor in the presence of an external magnetization. Given that proximity-induced chiral superconductivity recently led to one-dimensional Majorana fermion modes in the hybrid system of a magnetic topological insulator thin film coupled to a superconductor [33], a relevant question to address in this context might be the coexistence of chiral  $p$ -wave superconductivity (which is intrinsic in our case) with a Quantum Anomalous Hall state, induced by the external magnetization, on the surface of  $\text{Pb}_{1-x}\text{Sn}_x\text{Te}$ .

SK acknowledges Debjyoti Burdhan for his help with some of the figures. VT acknowledges DST for a Swarnajayanti grant (No. DST/SJF/PSA-0212012-13).

---

[1] L. Fu, Phys. Rev. Lett. **106**, 106802 (2011).  
 [2] P. Dziawa, B. Kowalski, K. Dybko, R. Buczko, A. Szczerbakow, M. Szot, E. Łusakowska, T. Balasubramanian, B. M. Wojek, M. Berntsen, *et al.*, Nat. Mater. **11**, 1023

(2012).  
 [3] T. H. Hsieh, H. Lin, J. Liu, W. Duan, A. Bansil, and L. Fu, Nat. Commun. **3**, 982 (2012).  
 [4] Y. Tanaka, Z. Ren, T. Sato, K. Nakayama, S. Souma, T. Takahashi, K. Segawa, and Y. Ando, Nature Phys. **8**, 800 (2012).  
 [5] S.-Y. Xu, C. Liu, N. Alidoust, M. Neupane, D. Qian, I. Belopolski, J. Denlinger, Y. Wang, H. Lin, L. Wray, *et al.*, Nat. Commun. **3**, 1192 (2012).  
 [6] J. Liu, W. Duan, and L. Fu, Phys. Rev. B **88**, 241303 (2013).  
 [7] H. Yao and F. Yang, Phys. Rev. B **92**, 035132 (2015).  
 [8] I. Dzyaloshinskii, JETP Lett. **46** (1987).  
 [9] I. Dzyaloshinskii, J. Phys. I **6**, 119 (1996).  
 [10] M. Baranov, A. Chubukov, and M. YU. KAGAN, IJMPB **6**, 2471 (1992).  
 [11] B. A. Bernevig, T. L. Hughes, and S.-C. Zhang, Science **314**, 1757 (2006).  
 [12] J. González, F. Guinea, and M. Vozmediano, Europhys. Lett. **34**, 711 (1996).  
 [13] C. Honerkamp and M. Salmhofer, Phys. Rev. Lett. **87**, 187004 (2001).  
 [14] J. L. McChesney, A. Bostwick, T. Ohta, T. Seyller, K. Horn, J. González, and E. Rotenberg, Phys. Rev. Lett. **104**, 136803 (2010).  
 [15] M. R. Norman, Science **332**, 196 (2011).  
 [16] V. P. Mineev, K. Samokhin, and L. Landau, *Introduction to unconventional superconductivity* (CRC Press, 1999).  
 [17] M. Sigrist and K. Ueda, Rev. Mod. Phys. **63**, 239 (1991).  
 [18] N. Furukawa, T. Rice, and M. Salmhofer, Phys. Rev. Lett. **81**, 3195 (1998).  
 [19] R. Nandkishore, L. Levitov, and A. Chubukov, Nature Phys. **8**, 158 (2012).  
 [20] J.-Q. Huang, C.-H. Hsu, H. Lin, D.-X. Yao, and W.-F. Tsai, Phys. Rev. B **93**, 155108 (2016).  
 [21] K. Le Hur and T. M. Rice, Ann. Phys. **324**, 1452 (2009).  
 [22] S. Kundu and V. Tripathi, arXiv preprint arXiv:1704.07437 (2017).  
 [23] M. Serbyn and L. Fu, *Physical Review B*, **90** (2014).  
 [24] C.-Y. Huang, H. Lin, Y. J. Wang, A. Bansil, and W.-F. Tsai, Physical Review B **93**, 205304 (2016).  
 [25] J. Liu, T. H. Hsieh, P. Wei, W. Duan, J. Moodera, and L. Fu, arXiv preprint arXiv:1310.1044 (2013).  
 [26] C. Fang, M. J. Gilbert, and B. A. Bernevig, Phys. Rev. Lett. **112**, 046801 (2014).  
 [27] S.-Y. Xu, M. Neupane, C. Liu, D. Zhang, A. Richardella, L. A. Wray, N. Alidoust, M. Leandersson, T. Balasubramanian, J. Sánchez-Barriga, *et al.*, arXiv preprint arXiv:1212.3382 (2012).  
 [28] A. Chubukov, Physica C **469**, 640 (2009).  
 [29] K. Michaeli and L. Fu, Phys. Rev. Lett. **109**, 187003 (2012).  
 [30] Y. Nagai, Physical Review B **91**, 060502 (2015).  
 [31] A. P. Mackenzie, R. K. W. Haselwimmer, A. W. Tyler, G. G. Lonzarich, Y. Mori, S. Nishizaki, and Y. Maeno, Phys. Rev. Lett. **80**, 161 (1998).  
 [32] S. Das, L. Aggarwal, S. Roychowdhury, M. Aslam, S. Gayen, K. Biswas, and G. Sheet, Appl. Phys. Lett. **109**, 132601 (2016).  
 [33] Q. L. He, L. Pan, A. L. Stern, E. C. Burks, X. Che, G. Yin, J. Wang, B. Lian, Q. Zhou, E. S. Choi, *et al.*, Science **357**, 294 (2017).